Coefficients of Evaporation and Gas Phase Diffusion of Low-Volatility Organic Solvents in Nitrogen from Interferometric Study of Evaporating Droplets

ARTICLE *in* THE JOURNAL OF PHYSICAL CHEMISTRY A · FEBRUARY 2010

Impact Factor: 2.69 · DOI: 10.1021/jp911466e · Source: PubMed

Coefficients of Evaporation and Gas Phase Diffusion of Low-Volatility Organic Solvents in Nitrogen from Interferometric Study of Evaporating Droplets

D. Jakubczyk,* G. Derkachov, T. Do Duc, K. Kolwas, and M. Kolwas

Institute of Physics of the Polish Academy of Sciences, al. Lotników 32/46, 02-668 Warsaw, Poland

Received: November 05, 2009; Revised Manuscript Received: January 27, 2010

Evaporation of motionless, levitating droplets of pure, low-volatility liquids was studied with interferometric methods. Experiments were conducted on charged droplets in the electrodynamic trap in nitrogen at atmospheric pressure at 298 K. Mono-, di-, tri-, and tetra(ethylene glycols) and 1,3-dimethyl-2-imidazolidinone were studied. The influence of minute impurities (<0.1%) upon the process of droplet evaporation was observed and discussed. The gas phase diffusion and evaporation coefficients were found from droplet radii evolution under the assumption of known vapor pressure. Diffusion coefficients were compared with independent measurements and calculations (in air). Good agreement was found for mono- and di(ethylene glycols), and for 1,3-dimethyl-2-imidazolidinone, which confirmed the used vapor pressure values. The value of equilibrium vapor pressure for tri(ethylene glycol) was proposed to be 0.044 ± 0.008 Pa. The evaporation coefficient was found to increase from 0.035 to 0.16 versus the molecular mass of the compound.

1. Introduction

Emission of chemicals into the air raises various health and ecological concerns and requires proper management. There exist established procedures for calculation of environmental fates of individual compounds. The WATER9 computer program[1] is a good example. Such procedures require various input parameters, among others, saturated (equilibrium) vapor pressure and gas phase diffusion coefficient of the compound which are chiefly responsible for the evaporation rate of a compound.

There are several methods of measuring the equilibrium vapor pressure (see ref 2 and references therein). Some of them, like gas saturation techniques, gas chromatography, or methods based on relative volatilization rate measurement (e.g., thermogravimetry), are suitable for the low-pressure region (reportedly even down to 10^{-8} Pa). However, for many organic compounds, data in this region are still scarce and sometimes encumbered with significant uncertainty.

There are also several experimental methods of finding the gas phase diffusion coefficient (see refs 3 and 4 and references therein). For example there are gas chromatographic broadening and flow perturbation techniques,[5] twin-bulb method, Stefan tube method, thermal wave interference,[6] and many others. All these methods are essentially indirect. There are also several theoretical equations for finding gas phase diffusion coefficient (see ref 5 and references therein): Chapman−Enskog, Arnold−Gilliland, Chen−Othmer, Fuller−Schettler−Giddings and others. Since for many compounds the experimental data are not available, these equations are readily used.

Since chemicals often get into the air in the form of mist, a detailed consideration of the kinetics of evaporation of a small droplet is desirable. This in turn requires the introduction of still another parameter. The experimentally observed evaporation rate in the kinetic (ballistic) regime is usually smaller than theoretically allowed by the kinetic theory of gases. In order to reconcile the experimental findings with the predictions of the theory, Knudsen[7] introduced the evaporation coefficient, defined as the probability of crossing the interface by a molecule impinging on it. Though conceptually seemingly simple, this coefficient turned out to be quite difficult to measure. Though it is agreed that there is a barrier at the gas−liquid interface, its nature has not been thoroughly understood yet (see, e.g., 8−11). The results obtained for water over nearly a century, spanning from ∼0.001 to 1, make a striking example (see refs 12−15 for reviews). The measurements for other vapor−liquid systems are fewer and similarly nonconclusive. Adsorption of heterogeneous vapors on liquid water seems to attract more attention (see refs 16−21) than single-component evaporation/condensation (see ref 22 and references therein, and refs 11 and 23−25).

In our previous works (see ref 26 and references therein), we developed a method of finding the evaporation coefficient under the assumption of known equilibrium vapor pressure and gas phase diffusion coefficient. This method can be classified as a relative volatilization rate measurement. The results we obtained for water versus temperature are in excellent agreement with those obtained with a fundamentally different method of Boston College/Aerodyne Research Inc. group, described, e.g., in ref 27. In our method, droplet radii evolutions were obtained with a technique of Mie scattering imaging and were studied within the framework of the Maxwellian quasi-stationary evaporation model and kinetic theory of gases.[12,26,28] For slowly evaporating compounds the evaporation model is relatively simple and both gas phase diffusion and evaporation coefficients can be found under the assumption of known equilibrium vapor pressure. If the diffusion coefficient is known, it is also possible to work backward and find the equilibrium vapor pressure.

In the present work, we measured the evaporation and gas phase diffusion coefficients versus the properties (type) of liquid at constant temperature and pressure. We applied our method to a sequence of glycols: ethylene glycol (EG), di(ethylene glycol) (DEG), tri(ethylene glycol) (TEG) and tetra(ethylene glycol) (TTEG), and to 1,3-dimethyl-2-imidazolidinone (DMI). Glycols have a wide range of applications. They are used in chemical industry[29,30] as intermediates for a variety of products, capitalizing on their hygroscopicity, lubricity, and low volatility, such as resins, deicing fluids, heat transfer fluids, automotive antifreeze and coolants, adhesives, paints, electrolytic capacitors,

* To whom correspondence should be addressed, jakub@ifpan.edu.pl.

10.1021/jp911466e
Published on Web 02/18/2010

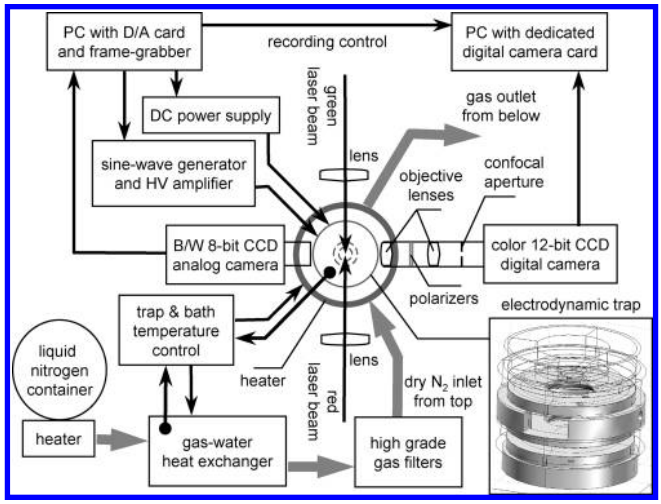

Figure 1. Experimental setup schematic view (top view, droplet injector omitted). Inset: electrodynamic trap drawing (wire-frame partially rendered).

textile fibers, paper, and leather. TEG and TTEG are also used as desiccants for gas purification[31] and in the production of theatrical smoke.[32] This last application requires dispensing them in aerosol form in quite large quantities. DMI is used, for instance, as a carrier for the black ink in jet printers, so globally also in significant quantities.

First we found the gas phase diffusion and evaporation coefficients. The diffusion coefficients were compared with experimental values, when known, and with the estimations made with the semiempirical equation from ref 33. Since the discrepancies for the two most slowly evaporating compounds (TEG and TTEG) were outside the estimated median error of the correlation, we tried to find the values of their equilibrium vapor pressures assuming diffusion coefficients predicted by the equation mentioned above.

2. Experimental Section

The experimental setup is presented in Figure 1. It consisted of a double-ring type electrodynamic quadrupole trap (inset in the Figure 1; see, e.g., refs 34 and 35) kept in a small ($\sim$ 10 cm^3) thermostatic chamber at 298 $\pm$ 0.1 K. Droplets were introduced into the trap through the top port with a piezo injector (described in detail in ref 36) kept inside the chamber. Thus, the initial temperature of the droplet was equal to that of the chamber. The initial droplet radius, at which we started the observation, was 9 $\pm$ 4 μm. Usually we were able to follow the evolution for a few micrometers, sometimes (depending on a substance used) as low as down to $\sim$650 nm. The upper and lower limit is primarily determined by the stability of the trap and the numerical aperture of the observation optics. Before the injection of each droplet, the chamber was flushed with filtered (H14 grade filter), dry nitrogen obtained by vaporizing liquid nitrogen. This procedure ensured that the gaseous environment into which the droplet was evaporating was void of aerosol, water, and eventual remnants from previous injections (liquid aerosol and solvent vapor). Apart from that, nitrogen atmosphere at standard temperature and pressure is relatively inert while its physical properties are close to those of air. The temperature of flowing nitrogen was matched ($\pm$0.2 K) to that of the trap by means of a gas$-$water thermostatic heat exchanger in order not to distract the thermostatic balance. Evaporation of a whole single droplet of several micrometer radius, in a chamber of the volume we used, gives rise to (average) vapor pressure several orders of magnitude ($\sim 10^8$ for TEG) below the corresponding equilibrium vapor pressure. The diffusion constants in nitrogen (air) of the organic solvents we used are comparatively high, which ensures uniform vapor density distribution. Thus, the presence of even several droplets does not influence the thermodynamic conditions in the chamber. However, lost droplets can get into the tight spaces of the trap, which after some accumulation can distort the trapping field. In order to avoid that, the trap and the chamber were dismantled and thoroughly cleaned every several hundred injections. Since the experiment was carried out near room temperature, we could not fully avoid the ubiquitous water vapor diffusing from the elements of chamber and trap. However, on a time scale of several minutes the effect of water vapor could be neglected (relative humidity <5%). The gas flow was stopped for the duration of measurement in order to ensure that the droplet was stationary with respect to the gaseous medium. The movement of gas versus the droplet can dramatically speed up the evaporation. This phenomenon is actually utilized in thermogravimetric measurements. An example of variation of rate of mass loss versus volumetric flow rate can be found, e.g., in ref 37.

In our experiments we used pure substances (purity for each lot stated in GC area % by the manufacturer): ethylene glycol, 99.9% (SPECTRANAL, GC, Riedel-de Haën); di(ethylene glycol), 99.99% (BioUltra, GC, Fluka); tri(ethylene glycol), 99.96% (BioUltra, anhydrous, GC, Fluka); tetra(ethylene glycol), 99.7% (puriss., GC, Fluka); 1,3-dimethyl-2-imidazolidinone, 99.7% (purum, GC, Fluka).

Individual droplet radius temporal evolution $a(t)$ was obtained by analyzing the angular distribution of scattered light irradiance within the framework of the Mie theory (angle-resolved static light scattering). This is a well established interferometric technique. Its variants (laser imaging for droplet sizing (ILIDS), interferometric particle imaging (IPI), Mie scattering imaging (MSI), interferometric Mie imaging (IMI), etc.) are used for particle sizing, e.g., in sprays (see, e.g., ref 38 and references therein). The variant of this technique that we developed is outlined in ref 39 and the details specific to this work are given below. Green (532.07 nm) p-polarized and red (654.25 nm) s-polarized laser beams of $\sim$10 mW power each (inside the trap) and $\sim$0.5 mm waist were used simultaneously for droplet illumination. Droplet heating and direct momentum transfer from the beam could be neglected. We recorded (up to $\sim$30 fps, 640 $\times$ 480 pixels, 12-bit, PixelFly color camera, pco.imaging) the scattering of both beams (see top inset in Figure 2). The field of view (circular) was centered at the azimuthal angle of 90 $\pm$ 0.1° and the elevation angle of 0 $\pm$ 0.3° and corresponded to $\pm$(16.24 $\pm$ 0.02°) in either direction. It was horizontally divided into halves with perpendicular (s and p) polarizers. Having attributed different polarizations to different colors enabled easy check of polarizer leaks (proper setup) and monitoring of depolarization. In the case of homogeneous droplets, light depolarization would indicate contamination with solid particles and require exclusion of such measurement. The sequence of out-of-focus images (droplet was in the focal point of the objective lens) was analyzed off-line with our software (written in MATLAB). Each image was integrated with a proper distribution function over the elevation angle to ensure better signal-to-noise ratio. The analysis was based on comparing the azimuthal distribution of irradiance observed in each image to the library of patterns obtained with the aid of Mie theory. Performing analysis for two polarizations simultaneously and for the whole $a(t)$ evolution rather than for separate points only,

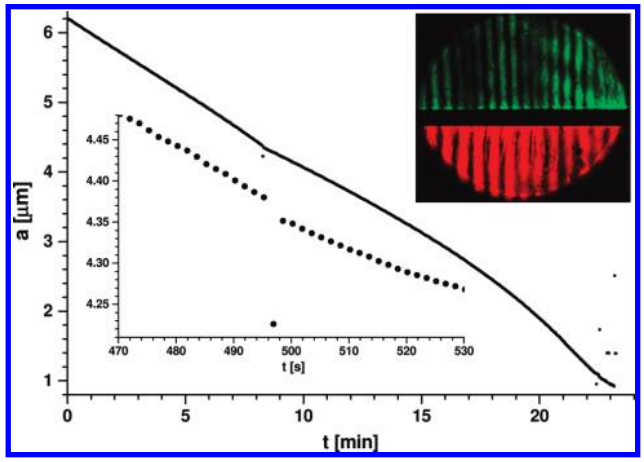

Figure 2. An example of TEG droplet radius temporal evolution. Each black dot represents a nonaveraged data point. Data points misinterpreted by the numerical method can be seen off the trend. Top inset: an example of a raw scattering image (frame). Bottom inset: magnification of a selected region of the main graph.

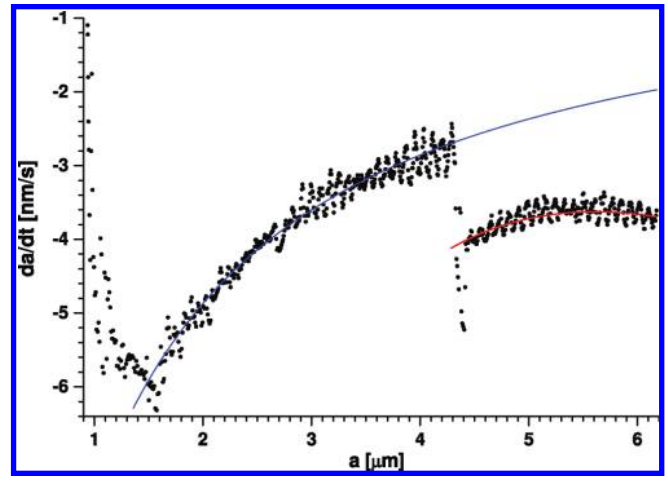

Figure 3. Droplet radius change rate versus droplet radius, corresponding to radius evolution from Figure 2. Experimental results are represented by black dots; fast oscillations are artifacts due to the averaging of digitized (high resolution) data. The $a > 4.4$ μm region is dominated by the evaporation of water, while in the $a < 1.5$ μm region the absolute value of da/dt diminishes rapidly due to the presence of low-volatility contaminants. For 1.5 μm $< a <$ 4.4 μm the evaporation of (nearly) pure TEG can be observed. The blue solid line represents the model fit for TEG evaporation, while the red line represents the fit for simultaneous TEG and water (two-component) evaporation.

enabled lifting some of the ambiguities associated with experimental uncertainties. The first procedure follows from the observation that the interference fringes corresponding to different polarizations shift in different direction versus a, while misalignment or/and distortion of the trapping field along the laser beams introduce systematic error to the azimuthal angle of observation and shift fringes in the same direction. The second procedure results from the observation that geometrical imperfections of the setup perpendicular to the laser beams introduce systematic error to the angular range of the field of view. This may cause large errors in readings of a but, fortunately, in a longer run it results in discontinuities in $a(t)$ and can be corrected by optimization. The later procedure also allows overcoming the difficulties in the interpretation of narrow resonances ($\leq$0.5 nm half-width at half-maximum, hwhm). Such resonances are very sensitive to many factors, like image integration over CCD exposition time or even slight droplet nonsphericity, which results in readings of a visibly off the trend. The average uncertainty of $a(t)$ was estimated from numerical experiments to be $\sim\pm$8 nm (compare bottom inset in Figure 2). It is due to several factors, of which we would like to address the main ones. The uncertainty of the refractive index is the most important among uncertainties of the parameters of the theory. For the compound lots we used, the manufacturer declared four significant digits of the refractive index, so the accuracy of $\pm$0.001 can be inferred. This, in average, corresponds to $\pm$3 nm uncertainty of $a(t)$. The maximal possible water content change of 0.03% corresponds (assuming rapid component mixing, see next section) to $\pm$0.1 nm uncertainty of $a(t)$. The total influence of the evaporation of volatile impurities (maximal content change of <0.3% (DMI,TTEG)) corresponds to less than $\pm$1 nm uncertainty of $a(t)$. Larger systematic errors of the refractive index (e.g., in the case of unreliable compound lot data) can be detected and corrected with the procedures described above. The angular resolution of a recorded image was (depending on the setup implementation) $\sim\pm$0.02°. This, in average, corresponds to $\pm$2 nm uncertainty of $a(t)$. Similar $a(t)$ uncertainty is associated with the uncertainty of the angular range of the field of view. The uncertainty was increasing in the vicinity of Coulomb explosions, which caused transient but large droplet nonsphericity (compare ref 40). Such an event, triggered by abrupt change of surface properties, can possibly be seen in Figure 2.

3. Evaporation Model

The quasi-stationary evaporation of a free (spherical), motionless droplet of a pure, low-volatility liquid, in an inert environment, can be adequately described with a relatively simple (mass transport) equation (compare, e.g., refs 12 and 41). It is convenient to write down this equation in a form describing the evolution of the droplet radius

$$\dot{a} \equiv \frac{\mathrm{d}a}{\mathrm{d}t} = -\frac{M}{R\rho}\frac{p_{\mathrm{sat}}(T)}{T}\frac{D\alpha}{a\alpha + D\sqrt{2\pi M/(RT)}} \qquad (1)$$

where a stands for the droplet radius, T is the ambient (and the droplet) temperature, p_{sat} is the equilibrium vapor pressure at a given temperature, D and α are gas phase diffusion and evaporation coefficient, respectively, ρ and M are the density and the molecular mass of the liquid, respectively, and R is the universal gas constant. This equation accounts both for diffusive transport (driven by the vapor density gradient) and for the kinetic (ballistic) transport in the very vicinity of the interface (below the distance of the mean free path of a molecule in the surrounding gaseous medium). Since the droplet was from 10 to 100 times larger than the mean free path in the surrounding gaseous medium, the influence of kinetic effects upon the evaporation was clearly recognizable but not dominating. The influence of the droplet curvature (surface tension) and of the droplet charge as well as of the transport of heat could be safely neglected for the droplets under consideration.

Since the experimental $a(t)$ dependence could also be represented in $\dot{a}(a)$ form, eq 1 did not require integration. Fitting eq 1 to the experimental $\dot{a}(a)$ yields simultaneously D and α (two-parameter fit, see blue line in Figure 3). In the case of extremely slowly evaporating TTEG (evolution up to 3 h), only the value of D could be inferred because of the relatively large fluctuations of $a(t)$.

However, even small amounts of impurities present in the liquids can change the evaporation scenario dramatically. Indeed, many of the droplet evolutions that we observed had to be

attributed to two- or three-component droplets (compare ref 42). The presence of nonvolatile impurities could be easily detected, since, due to the increase of their concentration during the evaporation process, the evolution slowed down at the end (Raoult's and Henry's laws). In this study we excluded this stage of evolution from the analysis. On the other hand, surprisingly small amounts of impurities of volatility significantly higher than that of the host medium/solvent (like water in glycol) manifested in visibly higher rate of evaporation at initial stage of evolution. In such a case of two-component evaporation, under assumption of rapid component mixing (shown in ref 42 to be in surprisingly good agreement with experimental data), eq 1 takes the form

$$\dot{a} \simeq \frac{-1}{RT\rho_{Lo}}\left[\frac{X_{Hi}(t)p_{satHi}(T)M_{Hi}D_{Hi}\alpha_{HiLo}}{a\alpha_{HiLo} + D_{Hi}\sqrt{2\pi M_{Hi}/(RT)}} + \frac{p_{satLo}(T)M_{Lo}D_{Lo}\alpha_{Lo}}{a\alpha_{Lo} + D_{Lo}\sqrt{2\pi M_{Hi}/(RT)}}\right] \quad (2)$$

where Hi and Lo indices pertain to high-volatility and low-volatility components, respectively (e.g., water and glycol). When the mole fraction of high-volatility component $X_{Hi} \ll 1$, the evaporation coefficient α_{HiLo} describes the interaction of a high-volatility vapor molecule with the low-volatility liquid surface. Since volatile liquids in general evaporate from the mixture sequentially (compare ref 42), it was possible (in all cases except TTEG, see below) to identify homogeneous domains of droplet radius evolution corresponding to two-component and single-component evaporation. Having the experimental data represented in derivative form $\dot{a}(a)$ greatly facilitated the analysis. A vivid example is presented in Figure 3, and the details of the analysis presented below pertain to this figure. We analyzed the single-component evaporation first by fitting eq 1 to the large homogeneous region directly preceding the evaporation slow-down (blue line in Figure 3). Then we introduced the obtained D_{Lo} and α_{Lo} into eq 2 in order to calculate $X_{Hi}(a)$ in a two-component region. Since the main volatile impurity was, according to the lot data, water, we assumed $D_{Hi} = D_w$ (H_2O in nitrogen, see ref 3) and approximated $\alpha_{HiLo} = \alpha_w$ (see ref 26). The resulting molar fraction of water could be well fitted with a second-order polynomial $X_w(a) = 3.1 \times 10^6(a - 4.4 \times 10^{-6})^2 + 1.5 \times 10^{-5}$ and, after introduction into eq 2, yielded the red line in Figure 3. This result seems to confirm that the rapid component mixing approximation is justified. However, it should be kept in mind that the physics behind this phenomenon may be different. The molar fraction of water at the very end of water evaporation should be much below the stationary value published by the manufacturer (0.026% by coulometric measurement). Indeed, we obtained $X_w(a = 4.4 \times 10^{-6}) \simeq 0.0016\%$, a value limited by the remnant humidity in the chamber and TEG high hygroscopicity. Since $X_{Hi}(t=0)$ is practically inaccessible in the experiments utilizing droplet injection (uncontrolled evaporation during the latency time before and after droplet injection, compare ref 42), the exact value of α_{HiLo} (e.g., water−TEG) could not be found.

4. Results and Discussion

The values of coefficients of diffusion in nitrogen under atmospheric pressure at 25 °C found in this study are presented in Figure 4 versus the calculated values (in air) as well as in Table 1. The coefficients of diffusion of EG, DEG, and TEG in air from ref 45 are also presented in Figure 4 and in Table 1. Table 1 also comprises the equilibrium vapor pressures from refs 29, 30, 43, and 44. For the calculation of coefficients of diffusion in air we used the semiempirical equation from ref 33. It is similar to the Arnold−Gilliland equation but with the molar volume estimated from the compound density only

$$D = 0.00229\frac{T^{1.5}M_{cor}\sqrt{0.034 + 1/M}}{\{[M/(2.5\rho)]^{1/3} + 1.8\}^2} \quad (3)$$

where

$$\begin{cases} M_{cor} = 1 - 0.000015M^2 & \text{for } M_{cor} < 0.4 \\ M_{cor} = 0.4 & \text{for } M_{cor} \geq 0.4 \end{cases}$$

The vertical error bars in Figure 4 represent statistical uncertainty (standard deviation) of experimentally found diffusion coefficients and the horizontal error bars represent the estimated median error of the correlation (7%[33]). As long as the diffusion coefficients we found under the assumption of known vapor pressure are in agreement with either the results of Lugg[45] or calculated values[33]), assuming that in nitrogen and in air they would be similar, it can be inferred that the values of vapor pressures taken from the literature were realistic.

However, for the two most slowly evaporating compounds (TEG and TTEG) the discrepancies were significant. In both cases the equilibrium vapor pressure value we used had been extrapolated from literature data corresponding to much higher

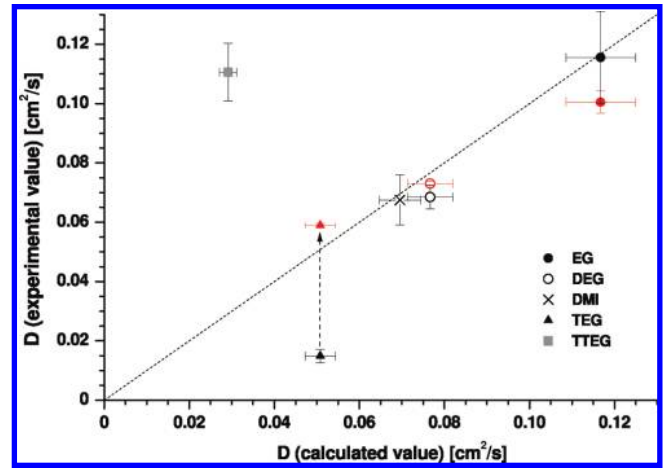

Figure 4. Coefficients of diffusion in nitrogen and air at 25 °C: measured versus calculated. Data from ref 45 shown in red. $D_{experimental} = D_{estimated}$ marked with dotted line. Proposed correction for TEG (see text) marked with arrow.

TABLE 1: Experimentally Obtained Values of Evaporation and Diffusion Coefficients: α and *D*, and Corresponding Vapor Pressure p_{sat}.[a]

liquid	α	*D* (mm² /s)	*D* (mm² /s)[45]	p_{sat} (Pa)
EG	0.035 ± 0.012	11.6 ± 1.6	10.05 ± 0.381	11.78[29]
DEG	0.082 ± 0.035	6.9 ± 0.4	7.3 ± 0.071	0.6263[30]
TEG (a)	0.16 ± 0.05	5.9 ± 0.06		0.044 ± 0.008
TEG (b)	0.017 ± 0.005	3.1 ± 1.3	5.9 ± 0.059	0.1743[43]
DMI	0.11 ± 0.04	6.8 ± 0.8		14.038[44]

[a] TEG (a) corresponds to p_{sat} we proposed. Data for the TTEG were not included as too tentative. Uncertainties represent standard deviations. Data for p_{sat} from refs 43 and 44 were extrapolated toward lower temperatures.

temperatures.[43,46,47] We considered it a probable source of errors. For instance, vapor pressure of DEG at 298 K, extrapolated from data in ref 47 (13.5 Pa), is an order of magnitude higher than extrapolated from the data from ref 46 (1.38 Pa). The value claimed as nonextrapolated, given in ref 30, is even lower (0.626 Pa). The accuracy of such extrapolation for TEG or TTEG can be even worse, since measurements were performed for temperatures a few tens of K higher than for DEG. Therefore, we assumed the diffusion coefficient of Lugg[45] and retrieved the value of the equilibrium vapor pressure working the evaporation model backward. Since our experimental data for TEG are of high accuracy, we believe that equilibrium vapor pressure we found at 298 K is quite accurate: 0.044 ± 0.008 Pa. It is lower than the extrapolated literature value[43,46,47] by a factor of $\sim$3. Similar procedure for TTEG was not possible, since we were not able to discern whether single-domain evolutions we observed did correspond to pure (single-component) TTEG evaporation. We were able to keep the humidity in the chamber low for several minutes but not hours. This was enough in case of the TEG evaporation, but very slowly evaporating hygroscopic liquid droplets, like those of TTEG, could absorb some water vapor.

The evaporation coefficients values found from our experiments are also presented in Table 1. They are of the order of the value we would expect at such temperature for water ($\alpha_w = 0.11$[26]). This can signify that low evaporation coefficient corresponding to a high interfacial barrier is not unique for water (compare $\alpha = 0.036$ for EG on H_2O[8,21]). There are very few references, that we know of, that we can compare our results with. In ref 11 we found $\alpha_{DEG} = 0.05$ and $\alpha_{TEG} = 0.46$ at 300 K. However, since the equilibrium vapor pressures used in ref 11 seems to be too high (see discussion above), after substituting the values we used/found one would get $\alpha_{DEG} \simeq 0.5$ and $\alpha_{TEG} \simeq 1$. This is closer to what can be found in ref 24 for DEG but much higher from what we obtained. It seems (see, e.g., ref 10 and references in refs 14 and 48) that experiments with evaporation of polar liquids into vacuum (see, e.g., unsteady state evaporation or jet stream tensimeter experiments) yield higher values of α than (quasi)equilibrium experiments.[15,26,49] On the other hand, much lower values of α_{EG} at 300 K can be found in ref 25 and the works cited therein. In those studies, a so-called, dropwise condensation method was used (compare ref 50 for water). This method yields $\alpha_{EG} \simeq 0.4$ at atmospheric pressure and $\alpha_{EG} \rightarrow 0.2$ for $p \rightarrow 0$.

The issue of evaporation into vacuum, essential also for understanding kinetics at the gas−liquid interface, has not been satisfactorily resolved yet (see, e.g., refs 51−55); however it seems that the application of the Hertz−Knudsen−Langmuir equation in its standard form may not be adequate in that case.

The values of evaporation coefficient we obtained, together with a previously obtained value for water,[26] were compared versus molecular mass, density, surface tension,[56] dipole moment, and dielectric constant[57] of the compound. The comparison yielded, except for water, a monotonic (approximately linear) dependence versus molecular mass, which is presented in Figure 5. There is also a hint of monotonic dependence versus density and dielectric constant for the series of glycols. The results are still too scarce to allow drawing any general conclusion about the physics behind them. The case of water may be special because of its unique bulk liquid and interfacial properties (see, e.g., 58−60 and references therein). However it is also possible that the value of the evaporation coefficient of water is off the trend because of a slightly different evaporation model was used.

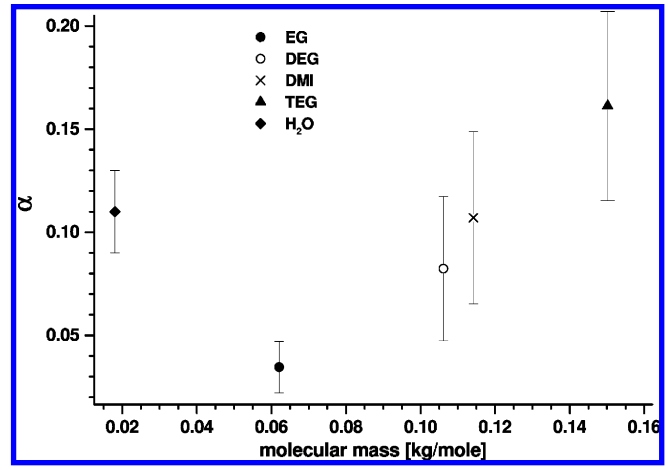

Figure 5. Evaporation coefficients found from our experiments (presented work and ref 26) versus molecular mass of the compound.

We intend to run experiments with other slowly evaporating liquids of diverse electrical properties and to try to clarify this issue.

5. Conclusions

The method we had originally developed for measuring the evaporation coefficient of water[26,41] was applied, after slight modification, to five slowly evaporating organic solvents in nitrogen at atmospheric pressure at 298 K and in the case of four of them (EG, DEG, TEG, and DMI) enabled measuring evaporation and diffusion coefficients. Good correlation between our measurements and independently measured (for EG and DEG) or estimated (for DMI) diffusion coefficients enabled verification of the equilibrium vapor pressure value used for each studied liquid. We proposed to correct the value of the equilibrium vapor pressure for TEG at 298 K to 0.044 ± 0.008 Pa. The evaporation coefficients were found to increase from 0.035 to 0.16 versus the molecular mass of the compound. According to our knowledge, our measurement of the evaporation coefficient of DMI is unique and the results for other liquids are of value since the literature data concerned is scarce and discussible. The influence of minute impurities (<0.1%) upon the process of droplet evaporation was observed and discussed.

The precision of droplet radius measurement was improved at least by a factor of 2, in comparison to mesurements reported in ref 26 and reached ± 8 nm or better, which opens opportunity for various precision measurements (e.g., small shape oscillations or small refractive index variations).

Acknowledgment. This work was supported by Polish Ministry of Science and Higher Education under Grant No. N N202 126837.

References and Notes

(1) *The Wastewater and Treatment Emissions Routines (WATER9), Version 2.0*, 2004, URL http://www.epa.gov/ttn/chief/software/water/index.html.
(2) Delle Site, A. *J. Phys. Chem. Ref. Data* **1997**, *26*, 157–193.
(3) Marrero, T.; Mason, E. *J. Phys. Chem. Ref. Data* **1972**, *1*, 1–118.
(4) Dutta, B. *Principles of mass transfer and separation processes*; PHI Learning Pvt. Ltd.: New Delhi, 2007.
(5) *Encyclopedia of chromatography*; Cazes, J., Ed.; Marcel Dekker: New York, 2001.
(6) Lima, J.; da Silva, M.; Sthel, M.; Cardoso, S.; Vargas, H.; Marin, E.; Miranda, L. *Rev. Sci. Instrum.* **2003**, *74*, 433–436.
(7) Knudsen, M. *The Kinetic Theory of Gases*; Methuen: London, 1950.

(8) Nathanson, G.; Davidovits, P.; Worsnop, D.; Kolb, C. *J. Phys. Chem.* **1996**, *100*, 13007–13020.
(9) Bagot, P.; Waring, C.; Costen, M.; McKendrick, K. *J. Phys. Chem. C* **2008**, *112*, 10868–10877.
(10) Drisdell, W.; Cappa, C.; Smith, J.; Saykally, R.; Cohen, R. *Atmos. Chem. Phys.* **2008**, *8*, 6699–6706.
(11) McFeely, F.; Somorjai, G. *Atmos. Chem. Phys. Discuss.* **1972**, *76*, 914–918.
(12) Pruppacher, H.; Klett, J. *Microphysics of Clouds and Precipitation*; Kluwer: Dordrecht, 1997.
(13) Marek, R.; Straub, J. *Int. J. Heat Mass Transfer* **2001**, *44*, 39–53.
(14) Eames, L.; Marr, N.; Sabir, H. *Int. J. Heat Mass Transfer* **1997**, *40*, 2963–2973.
(15) Davidovits, P.; Worsnop, D.; Jayne, J.; Kolb, C.; Winkler, P.; Vrtala, A.; Wagner, P.; Kulmala, M.; Lehtinen, K.; Vesala, T.; Mozurkewich, M. *Geophys. Res. Lett.* **2004**, *31*, L22111-1−4.
(16) Kirchner, W.; Welter, F.; Bongartz, A.; Kames, J.; Schweighoefer, S.; Schurath, U. *J. Atmos. Chem.* **1990**, *10*, 427–449.
(17) Rudolf, R.; Vrtala, A.; Kulmala, M.; Vesala, T.; Wagner, P. *Aerosol Sci.* **2000**, *32*, 913–932.
(18) Schwartz, S.; Freiberg, J. *Atmos. Environ.* **1981**, *15*, 1129–1144.
(19) Shi, Q.; Davidovits, P.; Jayne, J.; Worsnop, D.; Kolb, C. *J. Phys. Chem. A* **1999**, *103*, 8812–8823.
(20) Worsnop, D.; Zahniser, M.; Kolb, C.; Gardner, J.; Watson, L.; Van Doren, J.; Jayne, J.; Davidovits, P. *J. Phys. Chem.* **1989**, *93*, 1159–1172.
(21) Jayne, J.; Duan, S.; Davidovits, P.; Worsnop, D.; Zahniser, M.; Kolb, C. *J. Phys. Chem.* **1991**, *95*, 6329–6336.
(22) Fuchs, N. *Evaporation and Droplet Growth in Gaseous Media*; Pergamon: London, 1959.
(23) Heideger, W.; Boudart, M. *Chem. Eng. Sci.* **1962**, *17*, 1–10.
(24) Lednovich, S.; Fenn, J. *AIChE J.* **1977**, *23*, 454–459.
(25) Tsurata, T.; Kato, Y.; Yasunobu, T.; Masuoka, T. *Trans. Jpn. Soc. Mech. Eng., B* **1994**, *60*, 508–514.
(26) Zientara, M.; Jakubczyk, D.; Kolwas, K.; Kolwas, M. *J. Phys. Chem. A* **2008**, *112*, 5152–5158.
(27) Li, Y.; Davidovits, P.; Shi, Q.; Jayne, J.; Kolb, C.; Worsnop, D. *J. Phys. Chem. A* **2001**, *105*, 10627–10634.
(28) Bohren, C.; Huffman, D. *Absorption and Scattering of Light by Small Particles*; Wiley: New York, 1998.
(29) *Ethylene Glycol Product Guide*; MEGlobal Group of Companies: London, 2008.
(30) *Diethylene Glycol Product Guide*; MEGlobal Group of Companies: London, 2005.
(31) Kohl, A.; Nielsen, R. *Gas purification*; Gulf Professional Publishing: Houston, TX, 1997.
(32) Pendergrass, S. *Am. Ind. Hyg. Assoc. J.* **1999**, *60*, 452–457.
(33) *User's guide for WATER9 software, Version 2.0.0*, 2001.
(34) Major, F.; Gheorghe, V.; Werth, G. *Charged Particle Traps*; Springer: Berlin, 2005.
(35) Davis, E.; Buehler, M.; Ward, T. *Rev. Sci. Instrum.* **1990**, *61*, 1281–1288.
(36) Jakubczyk, D.; Derkachov, G.; Bazhan, W.; Lusakowska, E.; Kolwas, K.; Kolwas, M. *J. Phys. D* **2004**, *37*, 2918–2924.
(37) Viswanathan, R.; Lakshmi Narasimhan, T.; Nalini, S. *J. Phys. Chem. B* **2009**, *113*, 8362–8368.
(38) Dehaeck, S.; van Beeck, J. *Exp. Fluids* **2008**, *45*, 823–831.
(39) Zientara, M.; Jakubczyk, D.; Derkachov, G.; Kolwas, K.; Kolwas, M. *J. Phys. D* **2005**, *38*, 1978–1983.
(40) Duft, D.; Achtzehn, T.; Müller, R.; Huber, B.; Leisner, T. *Nature* **2003**, *421*, 128.
(41) Jakubczyk, D.; Zientara, M.; Kolwas, K.; Kolwas, M. *J. Atmos. Sci.* **2007**, *64*, 996–1004.
(42) Wilms, J. Evaporation of Multicomponent Droplets Thesis, Universität Stuttgart, 2005.
(43) NIST Chemistry WebBook, NIST Standard Reference Database Number 69, http://webbook.nist.gov/chemistry/, 2005.
(44) Kneisl, P.; Zondlo, J. *J. Chem. Eng. Data* **1987**, *32*, 11–13.
(45) Lugg, G. *Anal. Chem.* **1968**, *40*, 1072–1077.
(46) Shcherbina, E.; Tenenbaum, A.; Matveev, V.; Grishchenko, N. *Chem. Technol. Fuels Oils* **1975**, *11*, 603–605.
(47) Gallaugher, A.; Hibbert, H. *J. Am. Chem. Soc.* **1937**, *59*, 2521–2525.
(48) Chekmarev, S. *AIChE J.* **1996**, *42*, 2467–2475.
(49) Narusawa, U.; Springer, G. *J. Colloid Interface Sci.* **1975**, *50*, 392–395.
(50) Shaw, R.; Lamb, D. *J. Chem. Phys.* **1999**, *111*, 10659–10663.
(51) Hołyst, R.; Litniewski, M. *J. Chem. Phys.* **2009**, *130*, 074707−1-6.
(52) Frezzotti, A.; Gibelli, L.; Lorenzani, S. *Phys. Fluids* **2005**, *17*, 012102-1−12.
(53) Carey, V.; Wemhoff, A. *Int. J. Thermophys.* **2004**, *25*, 753–786.
(54) Ford, I.; Lee, T.-L. *J. Phys. D* **2001**, *34*, 413–417.
(55) Bellomo, N.; Chiadò Piat, M. *Meccanica* **1975**, *10*, 57–60.
(56) *Comparative Solvents Data, JEFFSOL Alkylene Carbonates*; Huntsman Corporation, 1999.
(57) Ballistreri, F.; Fortuna, C.; Musumarra, G.; Pavone, D.; S., S. *ARKIVOC* **2002**, 54–64.
(58) Huang, C. *Proc. Natl. Acad. Sci. U.S.A.* **2009**, *106*, 15214–15218.
(59) Smith, J.; Cappa, C.; Messer, B.; Drisdell, W.; Cohen, R.; Saykally, R. *J. Phys. Chem. B* **2006**, *110*, 20038–20045.
(60) Vega, C.; Abascal, J.; Sanz, E.; MacDowell, L.; McBride, C. *J. Phys.: Condens. Matter* **2005**, *17*, S3283–S3288.

JP911466E